Pump to Stokes Waves Intensity Noise Transfer in Cascaded Brillouin Fiber Lasers

Junhe Zhou, Yves Jaouen, Lilin Yi, and Philippe Gallion

***Abstract*—We propose a frequency model to address the relative intensity noise (RIN) transfer in cascaded Brillouin fiber lasers (CBFLs). An efficient model is derived from the multiple-wave-equation based on perturbation theory. For the sake of illustration, a third-order CBFL is analyzed. The modeling results show that RIN transfer in CBFLs has the resonant frequency associated with the fiber length and decays as the frequency increases to the order of megahertz due to the walk-off effect.**

***Index Terms*—Brillouin lasers, relative intensity noise (RIN) transfer.**

I. Introduction

BRILLOUIN fiber lasers (BFLs) have drawn wide attention recently due to their low threshold and high efficiency. Among them, cascaded Brillouin fiber lasers (CBFLs) are able to provide multiple lasing wavelengths and are very useful in wavelength-division-multiplexing transmission [1], [2]. The generation of over 160 Brillouin lasing wavelengths with the assistance of erbium-doped fiber amplifiers was reported [3], and so were the static and dynamic behaviors of CBFLs [4]–[6].

It is well known that intensity noise can be a major noise source that degrades the performance of optical communication systems [7], and pump to signal noise transfer in BFLs is quite strong due to high gain coefficient although it can be offset by the wave walk-off. Relative intensity noise (RIN) transfer in BFLs [8], [9] with single lasing wavelength has already drawn attention. However, up to date, no model has been proposed to study the noise transfer in CBFLs, which are of greater concern in potential practical applications. Moreover, most of the theoretical works were performed by using a temporal domain model [8]. However, it is less efficient to solve the two-dimensional partial differential equations as compared with the frequency model [10], which transfers the equations into the one-dimensional ordinary differential equations. The frequency domain model for RIN transfer in Brillouin amplifiers has been validated via experimental demonstration [10]. Hence, we propose to extend the frequency model to cascaded Brillouin fiber ring lasers (CBFRLs). The Fabry–Pérot Brillouin fiber lasers can also be characterized by the similar procedures.

II. Theoretical Frame

The typical setup for the CBFRLs is illustrated in Fig. 1. In the fiber, the pump propagates codirectionally with the even order Stokes waves and counterdirectionally with the odd order ones. We will introduce the multiwave equations and incorporate the boundary condition into the matrix form solution.

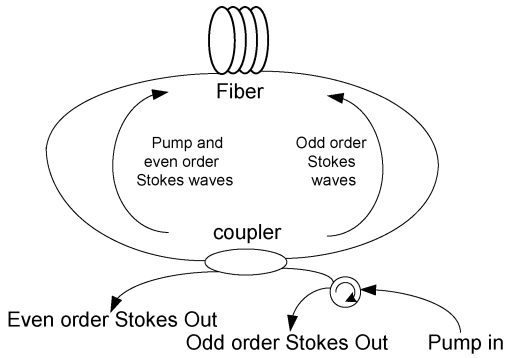

Fig. 1. Brillouin fiber ring laser scheme.

A. Multiwave Equations

The Brillouin scattering occurs with the interactions between the pump wave, Stokes wave, and the acoustic wave. For the CBFRLs, the wave equations are [11]

$$\begin{aligned}
&\frac{\partial E_1}{\partial z}+\frac{1}{V_g}\frac{\partial E_1}{\partial t}=-\frac{\alpha}{2}E_1-\frac{g_B}{2A}E_2Q_1\\
&\qquad\cdots\\
&\pm\frac{\partial E_i}{\partial z}+\frac{1}{V_g}\frac{\partial E_i}{\partial t}=-\frac{\alpha}{2}E_i+\frac{g_B}{2A}E_{i-1}Q_{i-1}^*-\frac{g_B}{2A}E_{i+1}Q_i\\
&\qquad\cdots\\
&\pm\frac{\partial E_N}{\partial z}+\frac{1}{V_g}\frac{\partial E_N}{\partial t}=-\frac{\alpha}{2}E_N+\frac{g_B}{2A}E_{N-1}Q_{N-1}^*\\
&\frac{\partial Q_i}{\partial t}+\frac{\Gamma_B}{2}Q_i=\frac{\Gamma_B}{2}E_iE_{i+1}^*
\end{aligned}\tag{1}$$

where E_i is the amplitude of the optical wave, Q_i the amplitude of the acoustic wave, g_B the Brillouin peak gain coefficient, A the effective area, Γ_B the phonon decay rate, α the fiber loss, and V_g the group velocity. $i=1$ stands for the pump wave, $i=2-N$ stands for the Stokes waves, and $+/-$ indicates the forward/backward wave propagation.

B. Frequency Domain Model

The amplitude E_i can be separated into its steady term and its noise term which are denoted as $E_i(z)$, $Q_i(z)$, $\Delta E_i(z,t)$, and $\Delta Q_i(z,t)$. The fluctuations are small as compared with the corresponding steady-state amplitudes. Substituting them into

Manuscript received October 19, 2007; revised January 30, 2008.

The authors are with École Nationale Supérieure des Télécommunications, (GET/Télécom Paris and CNRS UMR 5141LTCI), Paris 75013, France (e-mail: gallion@enst.fr).

Color versions of one or more of the figures in this letter are available online at http://ieeexplore.ieee.org.

Digital Object Identifier 10.1109/LPT.2008.922368

(1) and taking Fourier transform on the both sides, we have

$$\begin{aligned}
\frac{\partial \Delta\tilde{E}_1}{\partial z} - \frac{j\omega}{V_g}\frac{\partial \Delta\tilde{E}_1}{\partial t} &= -\frac{\alpha}{2}\Delta\tilde{E}_1 - \frac{g_B}{2A}\Delta\tilde{E}_2 Q_1 \\
&\quad - \frac{g_B}{2A}E_2\Delta\tilde{Q}_1 \\
&\cdots \\
\pm\frac{\partial \Delta\tilde{E}_i}{\partial z} - \frac{j\omega}{V_g}\frac{\partial \Delta\tilde{E}_i}{\partial t} &= -\frac{\alpha}{2}\Delta\tilde{E}_i + \frac{g_B}{2A}\Delta\tilde{E}_{i-1}Q^*_{i-1} \\
&\quad + \frac{g_B}{2A}E_{i-1}\Delta\tilde{Q}^*_{i-1} - \frac{g_B}{2A}\Delta\tilde{E}_{i+1}Q_i \\
&\quad - \frac{g_B}{2A}E_{i+1}\Delta\tilde{Q}_i \\
&\cdots \\
\pm\frac{\partial \tilde{E}_N}{\partial z} - \frac{j\omega}{V_g}\frac{\partial \tilde{E}_N}{\partial t} &= -\frac{\alpha}{2}\tilde{E}_N + \frac{g_B}{2A}\Delta\tilde{E}_{N-1}Q^*_{N-1} \\
&\quad + \frac{g_B}{2A}E_{N-1}\Delta\tilde{Q}^*_{N-1} \\
\left(\frac{\Gamma_B}{2} - j\omega\right)\Delta\tilde{Q}_i &= \frac{\Gamma_B}{2}\Delta\tilde{Q}_i E^*_{i+1} + \frac{\Gamma_B}{2}Q_i\Delta\tilde{E}^*_{i+1} \qquad (2)
\end{aligned}$$

where $\Delta\tilde{E}(z,\omega)$ and $\Delta\tilde{E}^*(z,-\omega)$ are the temporal Fourier transformations of $\Delta E(z,t)$ and $\Delta E^*(z,t)$. Equation (2) transforms the partial differential equations into the ordinary differential equations. The reduction of the two-dimensional problem into the one-dimensional one greatly saves the computational time. The later can be integrated by the numerical methods such as the Runge–Kutta method. The model is valid both in the pump undepleted and depleted regime [10].

C. Solution and Boundary Conditions

The significant difference between the models of BFLs and Brillouin amplifiers is that BFLs have the different boundary condition, which will be incorporated into the matrix form solution.

Rewriting (2) in the matrix form

$$\frac{\partial \Delta\tilde{\mathbf{E}}}{\partial z} = A(z)\Delta\tilde{\mathbf{E}} \qquad (3)$$

where $\Delta\tilde{\mathbf{E}} = (\Delta\tilde{E}_1, \Delta\tilde{E}^*_1, \cdots, \Delta\tilde{E}_N, \Delta\tilde{E}^*_N)^T$, A is the matrix whose components resulting from the corresponding terms in (2). The solution of (3) can be written as

$$\begin{aligned}
\Delta\tilde{\mathbf{E}}(L,\omega) &= \mathbf{M}_{\mathrm{RIN}}\Delta\tilde{\mathbf{E}}(0,\omega) \\
\mathbf{M}_{\mathrm{RIN}} &= \lim_{\Delta z\to 0}\prod_{k=1}^{L/\Delta z}(\mathbf{I} + \mathbf{A}(k\Delta z)\Delta z) \qquad (4)
\end{aligned}$$

where $\mathbf{I}$ is the identity matrix. For simplicity, we used the forward Euler method to represent $\mathbf{M}_{\mathrm{RIN}}$, but the more complicated and more efficient Runge–Kutta method may also be used.

The boundary condition can be written as

$$\begin{aligned}
\Delta\tilde{E}_1(0) &= \Delta\tilde{E}_1(L)\sqrt{R_1} + j\Delta\tilde{E}_{p0}\sqrt{1-R_1} \\
\Delta\tilde{E}_2(0) &= \Delta\tilde{E}_2(L)/\sqrt{R_2} \\
&\cdots \\
\Delta\tilde{E}_N(0) &= \begin{cases} \Delta\tilde{E}_N(L)\sqrt{R_N} & (N \text{ is odd}) \\ \Delta\tilde{E}_N(L)/\sqrt{R_N} & (N \text{ is even}) \end{cases} \qquad (5)
\end{aligned}$$

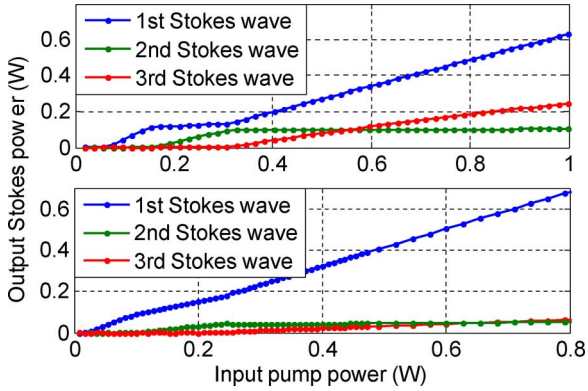

Fig. 2. The output power of Stokes waves as a function of input pump power (a) (The fiber length is 10 m and the coupling coefficient is 0.36.) (b) (The fiber length is 100 m and the coupling coefficient is 0.09.)

where R_i is the coupling coefficient of the coupler at the ith wavelength. Substituting (5) into (4), we have

$$\Delta\tilde{\mathbf{E}}(L,\omega) = (\mathbf{I} - \mathbf{M}_{\mathrm{RIN}}\mathbf{R})^{-1}\mathbf{M}_{\mathrm{RIN}}\mathbf{b} \qquad (6)$$

where $\mathbf{R}$ is a diagonal matrix $dig(\sqrt{R_1}, \sqrt{R_1}, 1/\sqrt{R_2}, 1/\sqrt{R_2}, \cdots)$, $\mathbf{b}$ is the RIN input vector $(j\Delta\tilde{E}_{p0}\sqrt{1-R_1}, -j\Delta\tilde{E}^*_{p0}\sqrt{1-R_1}, 0, 0\cdots)^T$.

When $\Delta\tilde{\mathbf{E}}(L,\omega)$ is obtained, we have

$$\Delta\tilde{\mathbf{E}}(0,\omega) = \mathbf{M}^{-1}_{\mathrm{RIN}}\Delta\tilde{\mathbf{E}}(L,\omega). \qquad (7)$$

The output RIN on even order Stokes waves can be obtained in the vector $\Delta\tilde{\mathbf{E}}(L,\omega)$, whereas the RIN on odd order Stokes waves can be found in $\Delta\tilde{\mathbf{E}}(0,\omega)$, respectively. The RIN transfer function is defined as $10log(\boldsymbol{r}_s/\boldsymbol{r}_p)$, where $r = (\boldsymbol{\Delta P}/\boldsymbol{P})^2$.

III. Results and Discussion

In our simulations, we consider RIN transfer in third-order CBFRLs. The gain medium is a dispersion-shifted fiber, with the following parameters: $A = 50\,\mu\mathrm{m}^2$, $g_B = 5\times10^{-11}$ m/W, and $\Gamma_B/2\pi = 40$ MHz. The coupling coefficients R_i are assumed to be wavelength-independent and the pump power coupled into the cavity is $(1-R)P_{p0}$. RIN transfer in third-order Brillouin scattering can be characterized by setting $N = 4$ (including the pump wave) in (2). The pump RIN is -100 dB. It is worth mentioning that the model shows excellent agreement with the time model for the first-order BFRLs.

Fig. 2 illustrates the output power of Stokes waves as a function of input pump power (the pump power refers to $(1-R)P_0$). In the upper subfigure, the fiber length is 10 m and the coupling coefficient is 0.36. The curves shown in the figure are in agreement with the ones in [4]. The pump power threshold to generate the first Stokes wave is reached first, and then the threshold for the second and the third Stokes waves. When the input pump power is far beyond the threshold, the first and the third Stokes waves are five and two times stronger than the second Stokes wave, respectively. We can also see that due to the high gain coefficient, the pump power is fully transferred to the Stokes waves indicating that the pump works in the depleted regime. In the second subfigure, the fiber length is 100 m and the coupling coefficient is 0.09. As the fiber length increases, the pump amplifies the Stokes waves during a longer fiber range, and therefore, the lasing threshold is much lower than the previous case.

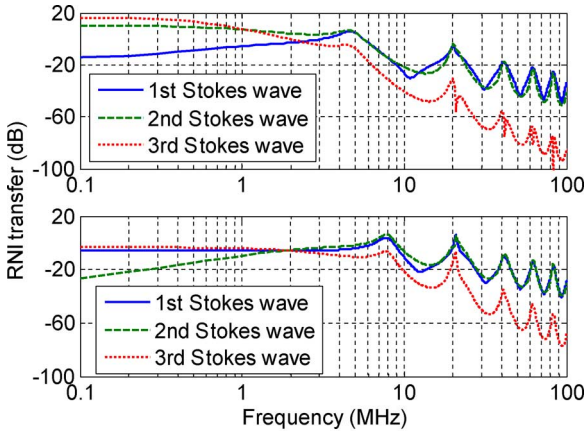

Fig. 3. (a) The input power pump is 40 mW. (b) The input power is 1 W.

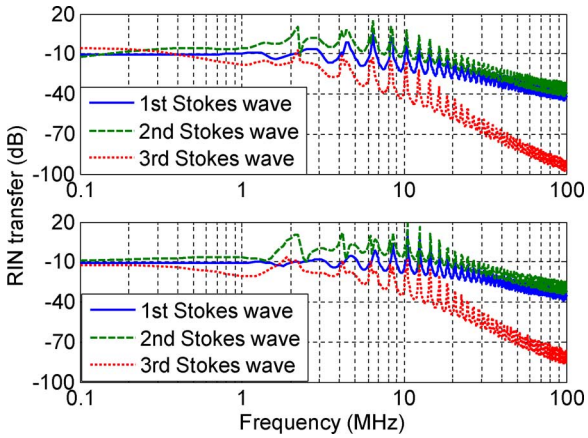

Fig. 4. The RIN transfer for the BFL with 100 m fiber, the coupling coefficient is 0.09. (a) The input pump power is 400 mW. (b) The input power is 800 mW.

From the slope of the curves, we can expect the first and the third Stokes waves to become stronger than the second Stokes wave as the input pump power grows.

Thereafter, we demonstrated the calculated RIN transfer function for each Stokes wave in Figs. 3 and 4. In Fig. 3, the fiber length is 10 m and the coupling coefficient is 0.36. We choose the pump power to be 0.4 W (for the first subfigure) and 1 W (for the second subfigure). At the low frequency, the walk-off effect is negligible and therefore, the RIN transfer remains constant. As the frequency increases, the RIN transfer shows oscillations due to the walk-off and the resonant effects. The resonant effect creates very high RIN transfer at resonant frequencies, at which the phase of the wave changes multiple π during one round-trip of propagation in the cavity

$$f_n = \frac{NV_g}{L}. \tag{8}$$

Substituting $L = 10$ m, $V_g = 2 \cdot 10^8$, $N = 1$ into (8), the first peak frequency can be roughly calculated as $2 \cdot 10^7$. From Fig. 3, we can see the frequency well agrees with the calculated one and it is independent of the input pump power. The shape of the RIN transfer curves on the first-order Stokes wave shown in Fig. 3 agrees with the experimental results in [9], which decays 20 dB/decade in the high frequency regime. The RIN transfer also decays 20 dB/decade on the second Stokes wave whereas it decays 40 dB/decade on the third Stokes wave in high frequency regime. This is because the pump, the first and second Stokes couples with each other directly in (2), however, the third-order Stokes wave couples with first and second Stokes waves only. We can also see that when the gain is fully saturated, i.e., when the input pump power is far beyond the threshold (the second subfigure), the RIN transfer is reduced.

In Fig. 4, the fiber length is changed to 100 m and the coupling coefficient is 0.09. The input pump power is 0.4 W (for the first subfigure) and 0.8 W (for the second subfigure). The second Stokes wave has the strongest RIN transfer function; this is because the first-order Stokes wave has the strongest power. The RIN transfer shows similar resonant effect as Fig. 3 as well. According to (8), since the fiber length is ten times longer than the previous one, the resonant frequencies are expected to be 1/10 as the ones shown in Fig. 3. It is illustrated as expected. Also, similarly, the walk-off effect strongly reduces the RIN transfer on the third Stokes wave at high frequency.

IV. Conclusion

We have proposed a frequency model to address the RIN transfer in CBFLs. The ordinary differential equations are derived in the frequency domain and the boundary conditions are incorporated into the matrix form solution. The method is capable of computing RIN transfer in CBFLs with arbitrary order Stokes waves with higher efficiency than the time domain model. As an example, numerical simulations are performed to study the RIN transfer in a third-order CBFRL. Simple formula is found to calculate the RIN transfer peak at resonant frequencies.

References

[1] K. O. Hill, B. S. Kawasaki, and D. C. Johnson, "CW Brillouin laser," *Appl. Phys. Lett.*, vol. 28, pp. 608–609, May 1976.

[2] L. F. Stokes, M. Chodorow, and H. J. Show, "All-fiber stimulated Brillouin ring laser with submilliwatt pump threshold," *Opt. Lett.*, vol. 7, pp. 509–511, Oct. 1982.

[3] L. Zhan, J. H. Ji, J. Xia, S. Y. Luo, and Y. X. Xia, "160-line multiwavelength generation of linear cavity self-seeded Brillouin-Erbium fiber laser," *Opt. Express*, vol. 14, pp. 10233–10238, 2006.

[4] K. Ogusu, "Analysis of steady-state cascaded stimulated Brillouin scattering in a fiber Fabry–Pérot resonator," *IEEE Photon. Technol. Lett.*, vol. 14, no. 7, pp. 947–949, Jul. 2002.

[5] S. Randoux, V. Lecoeuche, B. Ségard, and J. Zemmouri, "Dynamical behavior of a Brillouin fiber ring laser emitting two Stokes components," *Phys. Rev. A*, vol. 52, pp. 2327–2334, Sep. 1995.

[6] K. Ogusu and A. Sakai, "Generation and dynamics of cascaded stimulated Brillouin scattering in a high-finesse fiber Fabry–Pérot resonator," *Jpn. J. Appl. Phys.*, vol. 41, pp. 609–616, 2002.

[7] C. R. S. Fludger, V. Handerek, and R. J. Mears, "Pump to signal RIN transfer in Raman fiber amplifiers," *J. Lightw. Technol.*, vol. 19, no. 8, pp. 1140–1148, Aug. 2001.

[8] L. Stepien, S. Randoux, and J. Zemmouri, "Intensity noise in Brillouin fiber ring laser," *J. Opt. Soc. Amer.*, vol. B19, no. 5, pp. 1055–1066, May 2002.

[9] J. Geng and S. Jiang, "Pump-to-Stokes transfer of relative intensity noise in Brillouin fiber ring lasers," *Opt. Lett.*, vol. 32, pp. 11–13, 2007.

[10] J. Zhou, J. Chen, Y. Jaouën, L. Yi, X. Li, H. Petit, and P. Gallion, "A New frequency model for pump to signal RIN transfer in Brillouin fiber amplifiers," *IEEE Photon. Technol. Lett.*, vol. 19, no. 13, pp. 978–980, Jul. 1, 2007.

[11] G. P. Agrawal, *Nonlinear Fiber Optics*, 3rd ed. New York: Academic, 2001.